NANO LETTERS

pubs.acs.org/NanoLett

Reduction in the Thermal Conductivity of Single Crystalline Silicon by Phononic Crystal Patterning

Patrick E. Hopkins,[†] Charles M. Reinke,[†] Mehmet F. Su,[‡] Roy H. Olsson III,[†] Eric A. Shaner,[†] Zayd C. Leseman,[‡] Justin R. Serrano,[†] Leslie M. Phinney,[†] and Ihab El-Kady*[,†,‡]

[†]Sandia National Laboratories, Albuquerque, New Mexico 87185, United States, and [‡]University of New Mexico, Albuquerque, New Mexico 87131, United States

ABSTRACT Phononic crystals (PnCs) are the acoustic wave equivalent of photonic crystals, where a periodic array of scattering inclusions located in a homogeneous host material causes certain frequencies to be completely reflected by the structure. In conjunction with creating a phononic band gap, anomalous dispersion accompanied by a large reduction in phonon group velocities can lead to a massive reduction in silicon thermal conductivity. We measured the cross plane thermal conductivity of a series of single crystalline silicon PnCs using time domain thermoreflectance. The measured values are over an order of magnitude lower than those obtained for bulk Si (from 148 W m^{-1} K^{-1} to as low as 6.8 W m^{-1} K^{-1}). The measured thermal conductivity is much smaller than that predicted by only accounting for boundary scattering at the interfaces of the PnC lattice, indicating that coherent phononic effects are causing an additional reduction to the cross plane thermal conductivity.

KEYWORDS Phononic crystal, thermal conductivity, phonon transport, incoherent vs. coherent effects

Silicon is at the heart of almost all hi-tech devices and applications. It is arguably the seed of the semiconductor revolution. One of the fundamental tenets for silicon electronics is controlling the heat flow that is a byproduct of the nature of electronic operations. While ultralow thermal conductivity has been observed in silicon nanowires and nanomeshes, the fundamental barriers remain against the practical implementation of such ultrasmall devices. Here, we report on a successful methodology implementing a phononic crystal geometry in silicon that results in the same order of magnitude of thermal conductivity reduction as silicon nanowires while maintaining the characteristic length scales at an order of magnitude larger. Since phononic crystals can be mass produced and are compatible with standard CMOS fabrication, this enables the practical implementation of such devices. An added bonus of this approach comes to light by realizing that the electron mean free path is an order of magnitude smaller than that of the phonons involved, thereby possibly laying the foundation for the realization of exceptionally high ZT (thermoelectric figure of merit) in silicon and other phononic crystal (PnC) amenable material systems.

In general, material systems with structural length scales on the order of nanometers have unique abilities to control thermal transport.[1] Internal interfaces and boundaries in nanosystems create thermal carrier scattering events, and tailoring the period or structure of these boundaries offers a unique method for tuning their thermal properties. While this aspect of reducing the thermal conductivity alone has resulted in ultralow thermal conductivity of fully dense materials[2,3] which proves useful for thermal barrier applications,[4] this "boundary engineering" has also proven successful in designing nanocomposites for thermoelectric applications.[5] The efficiency of material systems for thermoelectric applications can be quantified with the well-known nondimensional thermoelectric figure of merit, $ZT = S^2\sigma T\kappa^{-1}$, where T is the temperature, S is the Seebeck coefficient, σ is the electrical conductivity, and κ is the thermal conductivity. Therefore, introducing interfaces and boundaries at length scales that will scatter phonons more frequently than electrons will reduce the thermal conductivity more than the electrical conductivity, thereby increasing ZT.

This approach of nanoengineering material boundaries has been useful in decreasing the thermal conductivity of single crystalline silicon. Silicon nanowires have shown particular promise for low thermal conductivity applications through further reduction of nanowire diameter and increased surface roughness.[6−9] However, structural stability and large contact areas are necessary criteria for most applications, and individual nanowires lack both of these characteristics. Increasing the perpendicular contact area of individual nanowires causes single nanowires to lose their unique thermal properties, and creating large arrays of nanowires with appropriate lengths creates difficulties in nanowire alignment and integrity. Therefore, we propose a

* Corresponding author, ielkady@sandia.gov.
Received for review: 8/17/2010
Published on Web: 11/24/2010

DOI: 10.1021/nl102918q | *Nano Lett.* **2011,** *11,* 107–112

new parameter to evaluate the applicability of low thermal conductivity materials based on the usable area of the material of interest. This parameter, the thermal conductivity of a "unit cell" of a material, is given by $\kappa_{uc} = \kappa_m/A_{uc}$, where κ_m is the measured thermal conductivity of the nanosystems and A_{uc} is the minimum, repeatable cross sectional area of the solid matrix of the unit cell. Ideally, A_{uc} should be as large as possible so that κ_{uc} is minimized for low thermal conductivity applications. In the previously measured nanowires, A_{uc} is defined as the cross section area of the nanowire.

Following this logic, recent work by Yu et al.[10] studied the thermal conductivity of Si nanomesh films that were theorized to have phononic crystal properties. Phononic crystals are the acoustic wave equivalent of photonic crystals, where a periodic array of scattering inclusions located in a homogeneous host material causes certain frequencies to be reflected by the structure (for a review, see ref 11). The nanomeshes studied by Yu et al. exhibited thermal conductivities similar to those of the lowest thermal conductivity nanowires. These nanomeshes were able to be developed as films with a 100 μm^2 areal footprint, alleviating the aforementioned stability aspect of the nanowires, but the nanomesh films were only grown to ~20 nm film thicknesses. Therefore, the unit cell area as previously defined is still of the same order of magnitude as many of the Si nanowires. In the case of the nanomeshes, A_{uc} is defined as in-plane, cross sectional area of an individual ligament in the nanomesh, explicitly defined by Yu et al.[10]

In response to the previously mentioned research, in this work, we investigate the thermal conductivity of single crystalline silicon PnCs with a thickness of 500 nm, pore spacings of several hundreds of nanometers, and areal footprints of ~10000 μm^2. We measure the thermal conductivity in the cross plane direction of these PnCs with time domain thermoreflectance; this direction of thermal propagation exhibits A_{uc} nearly 3 orders of magnitude larger than that of the nanomeshes. Although the PnCs studied in this work have band gaps in the gigahertz regime, well below terahertz phonon frequencies known to affect thermal transport in silicon,[12] the periodic nature of the PnCs coherently alter the phononic spectrum, which affects the thermal conductivity. In addition, incoherent phonon scattering at the physical boundaries of the PnC lattice will also cause a reduction in the phonon thermal conductivity. We use this to describe the thermal conductivity reduction in the PnCs studied in this work by accounting for phonon scattering and dispersion changes in the specific PnCs examined in this study.

The fabrication of the PnC begins with 150 μm silicon-on-insulator (SOI) wafers, where the buried oxide (BOX) layer is 3 μm thick. The ⟨100⟩, n-type, top Si layer where the PnC devices are realized is 500 nm thick and has a resistivity of 37.5−62.5 $\Omega\cdot$cm. The PnCs are formed by etching circular air holes of diameter d = 300−400 nm in the top

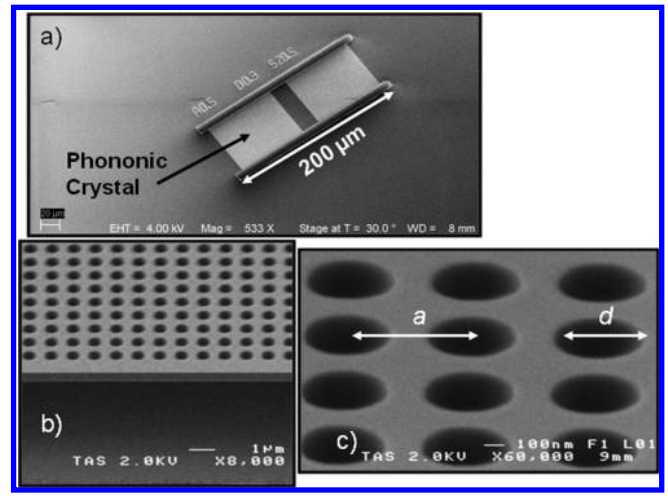

FIGURE 1. (a) Top-down image of a membrane containing two PnCs with a = 500 nm and d = 300 nm. The membrane is 60 μm wide and 200 μm long. A 20.5 μm wide area between the PnCs is located in the center of the membrane. The length of each PnC is 80 μm for a total of 160 periods. (b) Side image of a PnC membrane showing its suspension above the substrate. (c) Close in image of a Si/air PnC showing the lattice constant, a, and hole diameter, d. In the cross plane direction, these PnCs have solid matrix unit cell areas of $A_{uc} = a^2 - \pi d^2/4$.

Si, arranged in a simple cubic lattice, with center-to-center hole spacings, a, of 500, 600, 700, and 800 nm. The samples studied here specifically have: d/a = 300/500 nm (3/5), 300/600 nm (3/6), 400/700 nm (4/7), and 400/800 nm (4/8). In the cross plane direction, these PnCs have solid matrix unit cell areas of $A_{uc} = a^2 - \pi d^2/4$. Release areas are also etched in the top Si to the BOX, and the PnC membranes are suspended above the substrate by removing the BOX in vapor phase hydrofluoric acid (VHF). Figure 1a shows a top-down image of a membrane containing two PnCs with a = 500 nm and d = 300 nm. The membrane is 60 μm wide and 200 μm long and is comprised of two PnCs separated by a 20.5 μm wide unpatterned area. The length of each PnC is 80 μm for a total of 160 periods when a = 500 nm. The 600, 700, and 800 nm lattice constant devices have the same membrane width, length, and spacing between the PnCs and contain 133, 115, and 101 PnC periods, respectively, maintaining a nearly constant PnC length of 80 μm for each sample. Figure 1b shows a side image of a PnC membrane and its suspension above the substrate to isolate thermal effects in the membrane. Figure 1c shows a close in image of a Si/air PnC.

We measured the thermal conductivity of the PnCs with the time-domain thermoreflectance technique (TDTR).[13,14] Our specific experimental setup is described in detail in ref 15. TDTR is a noncontact, pump−probe technique in which a modulated train of short laser pulses (in our case ~100 fs) is used to create a heating event ("pump") on the surface of a sample. This pump−heating event is then monitored with a time-delayed probe pulse. The change in the reflectivity of the probe pulses at the modulation frequency of the pump train is detected through a lock-in amplifier; this change in

DOI: 10.1021/nl102918q | *Nano Lett.* **2011,** *11,* 107–112

reflectivity is related to the temperature change on the surface of the sample. These temporal temperature data are related to the thermophysical properties of the sample of interest. In practice, a thin metal film is deposited on the sample of interest which acts as a thermometer that absorbs the pump energy in less than 15 nm below the surface. In this study, we sputter 100 nm of Al on the surface of the PnCs. We monitor the thermoreflectance signal over 4.0 ns of probe delay time. The deposited energy takes ~100 ps to propagate through the Al layer, and the remaining 3.9 ns of delay time are related to the heat flow across the Al/PnC interface and through the PnC.

The thermoreflectance signal we monitor is the ratio of the in-phase to the out-of-phase voltage recorded by the lock-in amplifier. The ratio is related to the temperature change by

$$\text{ratio} = -\frac{\text{Re}[\sum_{M=-\infty}^{\infty} \Delta T(\omega_0 + M\omega_L) \exp[iM\omega_L\tau]]}{\text{Im}[\sum_{M=-\infty}^{\infty} \Delta T(\omega_0 + M\omega_L) \exp[iM\omega_L\tau]]} \quad (1)$$

where ΔT is the temperature rise on the sample surface, ω_0 is the pump modulation frequency, ω_L is the modulation frequency of the laser source, and τ is the pump−probe delay time. Our Ti:sapphire oscillator has a nominal repetition rate of 80 MHz. The thermal model and analysis used to predict ΔT is described in detail in refs 16 and 17. In short, the thermal model accounts for heat transfer in composite slabs[18] from a periodic, Gaussian source (pump) convoluted with a Gaussian sampling spot (probe).[16] In our experiments, our pump modulation frequency is 11 MHz and our pump and probe spot sizes are 15 μm. The temperature change at the surface is related to the thermal conductivity, κ, and heat capacity, C, of the composite slabs and the thermal boundary conductance, h_K, between each slab at a distance of

$$\delta = \sqrt{2\kappa/(C\omega_0)}$$

underneath the surface, where δ is the thermal penetration depth from the modulated pump train.

As h_K is highly dependent on the structure and material composition around the interface, for any given material system h_K can change from sample to sample.[19−21] Therefore, we deposit 100 nm of Al on the entire wafer including both the PnC structures and the areas without the PnCs. This allows us to independently measure h_K with TDTR at the deposited Al/Si interface without any complication from the PnC structure. (See Supporting Information for measurements and sensitivity analysis.) We measure h_K at the Al/Si material interfaces as 170 ± 20 MW m^{-2} K^{-1}. We then collect TDTR data on the four different PnC structures (3/5, 3/6, 4/7, and 4/8) at room temperature. The temporal decay of the thermoreflectance signal (which is related to the temperature change) is much different than that of the Si film used for h_K calibration (see Supporting Information). A more shallow decay in the thermoreflectance signal represents a longer thermal time constant, which implies a reduction in the thermal diffusivity. This qualitatively shows the change in the thermal diffusivity of the PnC structures compared to the unpatterned Si thin film. To quantify this, we account for the reduction in C and h_K due to surface porosity of the Al-coated PnC structure by multiplying the bulk values of C in the Al film and Si PnC and h_K at the Al/Si PnC interface by a factor of $(1 - \phi)$ where ϕ is the porosity; this effectively treats the air in the PnC as nonabsorbing so that our best fit thermal conductivities represent the thermal transport through only the solid matrix of the PnC. We take the bulk values of C from the literature[22] and take the "nonporous" h_K value from the previous measurement at the Al/Si interface in the non-PnC fabrication locations on the wafer. The porosities of the 3/5, 3/6, 4/7, and 4/8 structures are calculated based on the geometry of each structure, and are ϕ = 0.28, 0.19, 0.25, and 0.19, respectively. The measured thermal conductivities on the (3/5), (3/6), (4/7), and (4/8) PnC structures are 5.84 ± 1.3, 4.81 ± 1.0, 7.11 ± 1.8, and 6.58 ± 0.5 W m^{-1} K^{-1}, where the uncertainty represents the standard deviation among the best fit to three different data sets taken on three different samples with similar geometries (nine data sets total).

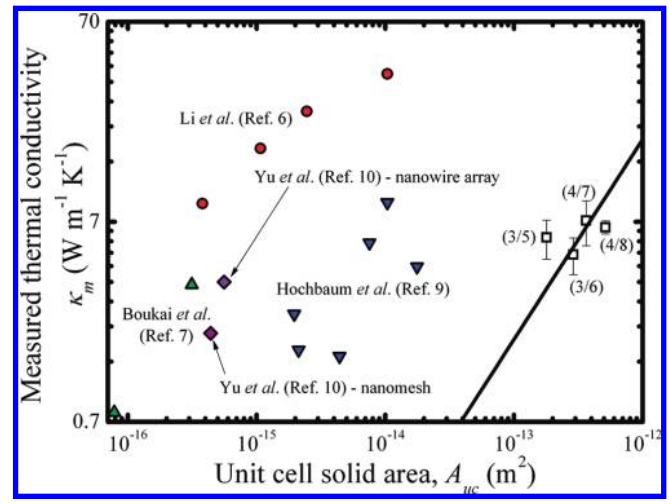

FIGURE 2. Measured thermal conductivity as a function of unit cell solid area. The four PnCs are depicted by the unfilled squares and the Si nanowires by the downward triangles,[9] upward triangles,[7] and circles.[6] The recent nanowire arrays and nanomesh data are depicted by the diamonds.[10] All data shown in this figure are for room temperature measurements except for the nanomesh data which was taken at 280 K. The solid lines represent $\kappa = \kappa_{uc\_PnC\_avg}A_{uc} = \kappa_{m\_PnC\_avg}A_{uc}/A_{uc\_PnC\_avg}$, where we calculate $\kappa_{m\_PnC\_avg}$ and $A_{uc\_PnC\_avg}$ by averaging values from the PnCs ($\kappa_{m\_PnC\_avg}$ = 6.09 W m^{-1} K^{-1} and $A_{uc\_PnC\_avg}$ = 0.337 μm^{-2}). The resulting κ_{uc} on the PnCs is the lowest κ_{uc} of any nanostructured Si material.

Figure 2 shows the measured thermal conductivity of the four PnCs as a function of unit cell area along with the

DOI: 10.1021/nl102918q | Nano Lett. 2011, 11, 107--112

measured thermal conductivity of the various Si nanostructures from previous studies. For the unit cell area of the PnCs, we subtract the area of the air holes to include only the unit cell of the solid fraction of the PnC. The thermal conductivities of the PnC structures show a drastic reduction from that of bulk, single crystalline Si (148 W m^{-1} K^{-1}).[22] Although the nanowires and nanomesh data show similar, if not greater reduction, the PnCs have a much greater (1−3 orders of magnitude) unit cell solid area than the nanowires for the same thermal conductivity. To directly compare the PnCs to the nanowire data, consider κ_{uc} on the PnCs extended to lower dimensions. The solid line in Figure 2 represents

$$\kappa = \kappa_{uc\_PnC\_avg} A_{uc} / A_{uc\_PnC\_avg}$$

where we calculate $\kappa_{m\_PnC\_avg}$ and $A_{uc\_PnC\_avg}$ by averaging values from the PnCs. This effectively projects the "device applicability" of the PnCs to lower unit cell areas. As apparent from Figure 2, κ_{uc} on the PnCs is the lowest κ_{uc} of any silicon nanostructured material ($A_{uc} < 10^{-12}$ m).

To understand the origin of this thermal conductivity reduction at room temperature, we turn to the Callaway-Holland-type model,[23,24] given by

$$\kappa = \frac{1}{6\pi^2} \sum_j \int_q C_j(q) v_j^2(q) \tau_j(q)\, dq \qquad (2)$$

where C_j is the specific heat per normal mode at frequency $\omega(q)$, v_j is the phonon velocity, τ_j is the scattering time, and q is the wavevector. In bulk Si, the scattering time around room temperature is dominated by Umklapp processes, with a relatively small contribution from impurity scattering. From Matthiessen's rule, the scattering time is given by $\tau_j(q) = (\tau_{U,j}^{-1}(q) + \tau_{I,j}^{-1}(q))^{-1}$, where the Umklapp scattering rate is given by $\tau_{U,j}^{-1}(q) = AT\omega^2(q) \exp[-B/T]$, where T is the temperature and A and B are coefficients to be determined, and the impurity scattering rate is given by $\tau_{I,j}^{-1}(q) = D\omega^4(q)$, where $D = 1.32 \times 10^{-45}$ s^3 (ref 24). We fit eq 2 to the measured thermal conductivity of bulk Si (ref 25), iterating A and B in the Umklapp scattering rate to achieve a best fit. From this, we determine that $A = 1.4 \times 10^{-19}$ s K^{-1} and $B = 152$ K. For these calculations, we use the dispersion of bulk Si by fitting a fourth degree polynomial to the dispersion calculated by Weber.[26] After determining the Umklapp scattering rate in Si, we then introduce a boundary scattering term via Matthiessen's rule to account for phonon scattering at the PnC pore boundaries given by $\tau_{B,j}^{-1}(q) = L/v_j(q)$, where L is the average distance between pore boundaries; note that this approach for modeling the reduction in thermal conductivity due to boundary scattering has proven successful in predicting the thermal conductivity of microporous,[27] polycrystalline,[28,29] and nanowire[30] silicon samples. For the PnCs of interest in this study, the pore edge to pore edge distances are 200, 300, 300, and 400 nm for the (3/5), (3/6), (4/7), and (4/8) structures, respectively.

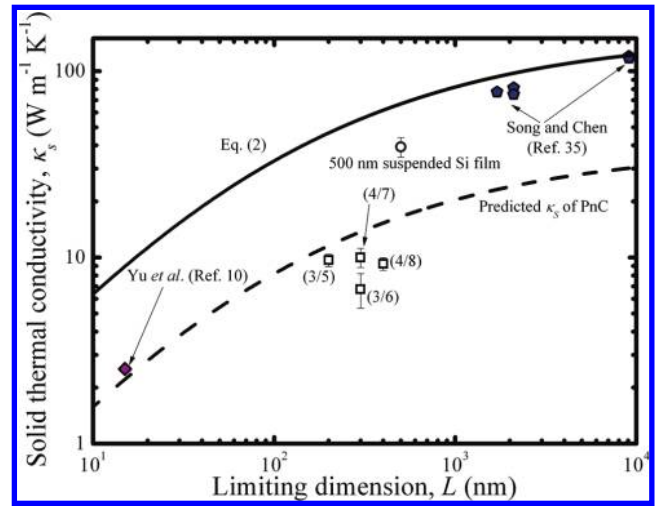

FIGURE 3. The thermal conductivity of Si structures at room temperature as a function of L for the PnCs (unfilled squares), microporous solids (filled pentagons),[35] nanomesh (filled diamond),[10] and a suspended 500 nm thick Si film—that is, an unpatterned Si slab (unfilled circle). The measured thermal conductivities of the porous structures are multiplied by a factor of $[(1 + 2\phi/3)/(1 - \phi)]$ to account for the porosity of the structures, and thereby directly compare the thermal conductivity of the solid matrix in the porous structures to the model in eq 2. The solid line represents predictions of eq 2 at room temperature as a function of L. Equation 2 predicts the thermal conductivity of the microporous solids well and only slightly overpredicts the thermal conductivity of the 500 nm suspended film. This model, however, drastically overpredicts the PnC measurements. The dashed line represents predictions of the PnC thermal conductivity, based on eq 2 with DOS calculations using the PWE method.

The thermal conductivity at room temperature as a function of L calculated via eq 2 is shown in Figure 3. Ultimately, we are interested in the thermal conductivity of the solid matrix in the PnC, not the reduction due to the removal of the material to create the PnC. To directly compare the thermal conductivity reduction of the solid material in the PnC to the reduction predicted from boundary scattering via eq 2, we use the expression derived by Eucken for the thermal conductivity of cylindrical porous solids.[31] Note that this expression has been used successfully to account for the reduction in thermal conductivity in microporous solids.[27] Following Eucken, the predicted thermal conductivity of the PnCs using eq 2 is related to the thermal conductivity of the solid matrix in the PnC through

$$\kappa_s = \kappa_m (1 + 2\phi/3)/(1 - \phi)$$

Although more rigorous treatments of porosity have been derived for nanoporous solids,[32,33] due to the large pore separation in our PnCs and relatively large porosities, we expect that the majority of the phonon modes will be scattered diffusively at the pore boundaries (i.e., the ballistic character of phonon transport and its interaction with the pore edges is not important)[34] and therefore the classical Eucken treatment should hold.

The thermal conductivities of the PnCs shown in Figure 3 as a function of pore-edge separation are the values from

DOI: 10.1021/nl102918q | *Nano Lett.* **2011,** *11,* 107–112

Figure 2 multiplied by the Eucken factor, where the porosities of the PnCs are 0.28, 0.20, 0.26, and 0.20 for the (3/5), (3/6), (4/7), and (4/8) structures, respectively. For comparison, we also include the measured thermal conductivity of the Si microporous solids measured by Song and Chen[35] and the nanomesh sample by Yu et al.,[10] also multiplied by the Eucken factor. Equation 2 predicts the thermal conductivity of the microporous solids well; however, this model overpredicts the measured PnC data by a factor of 5−7 and the data by Yu et al. by a factor of 4. The order of magnitude reduction in the PnC thermal conductivity compared to eq 2 can be ascribed to *the PnC periodically porous structure* changing the Si mode density. This shift in mode density can lead to a reduction in thermal conductivity. To verify this, we measure the thermal conductivity of suspended, unpatterned Si slabs (i.e., suspended Si slabs described earlier without PnC patterning). The slabs, which are 500 nm thick, are measured and analyzed via the TDTR procedure described earlier. The thermal conductivity of the 500 nm suspended Si film is 39.2 ± 4.8 W m^{-1} K^{-1}, as shown in Figure 3; the limiting dimension of this suspended film is 500 nm since the suspended film boundary forces phonon scattering at a distance of 500 nm below the surface. The thermal conductivity of the suspended, upatterned film, which is only slightly overpredicted by eq 2, is nearly a factor of 3−4 higher than the PnC data which has a similar limiting spacing. This further shows that the coherent, phononic effect in the PnCs is causing an additional reduction in the phononic thermal conductivity beyond the effect from boundary scattering alone.

To investigate this effect further, we implemented the plane-wave expansion (PWE) technique[36] to calculate the phononic density of states (DOS) of the PnC from its dispersion and used these data to calculate the change in thermal conductivity of the PnC as compared to bulk (i.e., unpaterened) Si. The PWE model is solved for the eigenmodes of an infinite 2D PnC structure. Such a model accurately matches the behavior of the experimental measurements, since the thermal waves excited by the modulated pump propagate only a very short depth into the PnC slab due to the high repetition rate (11 MHz) used in the TDTR experiments and thus do not "see" the finite thickness of the sample. The DOS of a given structure is calculated by numerically integrating the number of modes with respect to frequency for all directions in the first 2D Brillouin zone. Figure 4 shows the integrated density of states as a function of frequency for bulk Si and a PnC with $d/a = 0.6$ (the bulk dispersion was calculated using the same material parameters as the PnC but with $d/a = 0$). The inset shows the calculated density of states of the PnC. The observed spike in the low frequency modes is indicative of a large reduction in the phonon group velocity in the PnC lattice.

Once the DOS was found, the thermal conductivity was calculated via eq 2. The thermal conductivity of the PnC predicted from the PWE DOS versus L is shown in Figure 3

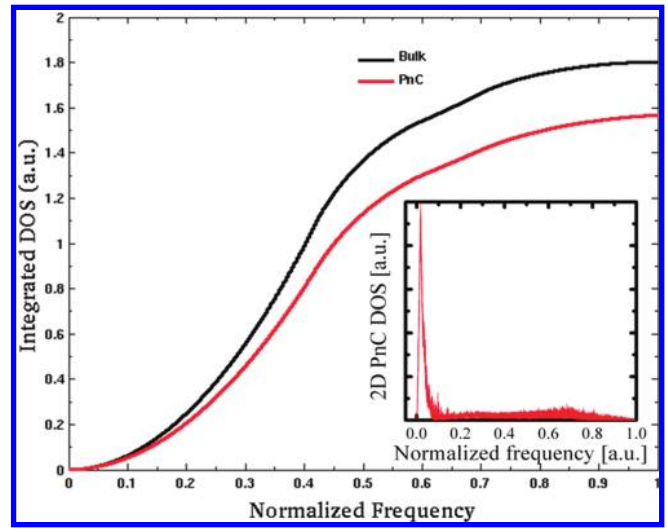

FIGURE 4. Integrated density of states as a function of frequency for bulk Si (black) and PnC lattice with $d/a = 0.6$ (red). The bulk dispersion was calculated using the same material parameters as the PnC but with $d/a = 0$. Inset shows the calculated density of states of the PnC. The observed spike in the low frequency modes is indicative of a large reduction in the phonon group velocity in the PnC lattice.

as a dashed line. The curve shows excellent agreement with the measured values from the PnC samples, particularly the 3/5 sample, which has the same pore radius as the value used in the simulations. The predictions also show excellent agreement with the thermal conductivity of Yu et al.'s nanomesh sample,[10] indicating that the further reduction observed in the PnC and nanomesh beyond that of eq 2 using a bulk dispersion is due to the changes in the mode density. This trend is based on calculations at smaller values of L, since the PWE technique becomes too computationally intensive for larger values of L to calculate the modal dispersion up to meaningful values using the resources available at the time of publication. This is directly related to the fact that thermal energy in Si follows a Bose−Einstein distribution, and thus the majority of the energy is carried by phonons in the 1−6 THz range.[12,27] Since the size of the PWE computational space grows nonlinearly with maximum mode frequency, this severely limits the largest lattice constant that can be simulated, as the frequency scales directly with the PnC lattice constant. However, the sound agreement between the predicted reduction in κ of the PnCs and that measured with TDTR elucidates the role of phonon dispersion and mode density on the further reduction in thermal conductivity of PnCs beyond that considering only boundary scattering effects.

In summary, we have experimentally studied the thermal transport processes in single crystalline silicon phononic crystals with submicrometer geometries. The measured values are over an order of magnitude lower than that of bulk Si, and for the structures in this work represent the lowest on thermal conductivity to solid area ratio of any silicon nanostructured material measured to date. The magnitude

DOI: 10.1021/nl102918q | *Nano Lett.* **2011,** *11,* 107–112

of this measured thermal conductivity reduction is much larger than that predicted from accounting for phonon–boundary scattering at the interfaces of the PnC lattice alone. To investigate the origin of this further reduction, we implemented the plane-wave expansion technique to calculate the phononic density of states of the PnC. The PnC density of states is drastically altered compared to bulk, and the predictions of the PnC thermal conductivity agree well with the experimental measurements, indicating that the thermal conductivity is drastically affected by the altered dispersion introduced by the periodically nanostructed nature of phononic crystals.

Acknowledgment. The authors are grateful for funding from the LDRD program office. P.E.H. is grateful for funding through the Sandia National Laboratories Harry S. Truman Fellowship. Sandia National Laboratories is a multiprogram laboratory managed and operated by Sandia Corporation, a wholly owned subsidiary of Lockheed Martin Corporation, for the U.S. Department of Energy's National Nuclear Security Administration under Contract DE-AC04-94AL85000.

Supporting Information Available. Additional information on phononic crystal fabrication, TDTR data analysis, and thermal conductivity modeling. This material is available free of charge via the Internet at http://pubs.acs.org.

REFERENCES AND NOTES

(1) Cahill, D. G.; Ford, W. K.; Goodson, K. E.; Mahan, G. D.; Majumdar, A.; Maris, H. J.; Merlin, R.; Phillpot, S. R. *J. Appl. Phys.* **2003**, *93*, 793–818.
(2) Chiritescu, C.; Cahill, D. G.; Nguyen, N.; Johnson, D.; Bodapati, A.; Keblinski, P.; Zschack, P. *Science* **2007**, *315*, 351–353.
(3) Costescu, R. M.; Cahill, D. G.; Fabreguette, F. H.; Sechrist, Z. A.; George, S. M. *Science* **2004**, *303*, 989–990.
(4) Padture, N. P.; Gell, M.; Jordan, E. H. *Science* **2002**, *296*, 280–284.
(5) Venkatasubramanian, R.; Siivola, E.; Colpittas, T.; O'Quinn, B. *Nature* **2001**, *413*, 597–602.
(6) Li, D.; Wu, Y.; Kim, P.; Shi, L.; Yang, P.; Majumdar, A. *Appl. Phys. Lett.* **2003**, *83*, 2934–2936.
(7) Boukai, A. I.; Bunimovich, Y.; Tahir-Kheli, J.; Yu, J.-K.; Goddard, W. A.; Heath, J. R. *Nature* **2008**, *451*, 168–171.
(8) Chen, R.; Hochbaum, A. I.; Murphy, P.; Moore, J.; Yang, P.; Majumdar, A. *Phys. Rev. Lett.* **2008**, *101*, 105501.
(9) Hochbaum, A. I.; Chen, R.; Delgado, R. D.; Liang, W.; Garnett, E. C.; Najarian, M.; Majumdar, A.; Yang, P. *Nature* **2008**, *451*, 163–167.
(10) Yu, J.-K.; Mitrovic, S.; Tham, D.; Varghese, J.; Heath, J. R. *Nat. Nanotechnol.* **2010**, *5*, 718–721.
(11) Olsson, R. H., III; El-Kady, I. *Meas. Sci. Technol.* **2009**, *20*, No. 012002.
(12) Henry, A. S.; Chen, G. *J. Comput. Theor. Nanosci.* **2008**, *5*, 1–12.
(13) Norris, P. M.; Caffrey, A. P.; Stevens, R. J.; Klopf, J. M.; McLeskey, J. T.; Smith, A. N. *Rev. Sci. Instrum.* **2003**, *74*, 400–406.
(14) Paddock, C. A.; Eesley, G. L. *J. Appl. Phys.* **1986**, *60*, 285–290.
(15) Hopkins, P. E.; Serrano, J. R.; Phinney, L. M.; Kearney, S. P.; Grasser, T. W.; Harris, C. T. *J. Heat Transfer* **2010**, *132*, No. 081302.
(16) Cahill, D. G. *Rev. Sci. Instrum.* **2004**, *75*, 5119–5122.
(17) Schmidt, A. J.; Chen, X.; Chen, G. *Rev. Sci. Instrum.* **2008**, *79*, 114902.
(18) Carslaw, H. S. Jaeger, J. C., Section 10.4.VI. The periodic point source. In *Conduction of Heat in Solids*, 2nd ed.; Oxford University Press: New York, 1959; p 263.
(19) Swartz, E. T.; Pohl, R. O. *Appl. Phys. Lett.* **1987**, *51*, 2200–2202.
(20) Hopkins, P. E.; Norris, P. M. *Appl. Phys. Lett.* **2006**, *89*, 131909.
(21) Hopkins, P. E.; Norris, P. M.; Stevens, R. J.; Beechem, T.; Graham, S. *J. Heat Transfer* **2008**, *130*, No. 062402.
(22) Incropera, F.; DeWitt, D. P. *Fundamentals of Heat and Mass Transfer*; Wiley and Sons, Inc.: New York, 1996.
(23) Callaway, J. *Phys. Rev.* **1959**, *113*, 1046–1051.
(24) Holland, M. G. *Phys. Rev.* **1963**, *132*, 2461–2471.
(25) Ho, C. Y.; Powell, R. W.; Liley, P. E. *J. Phys. Chem. Ref. Data* **1972**, *1*, 279–422.
(26) Weber, W. *Phys. Rev. B* **1977**, *15*, 4789–4803.
(27) Hopkins, P. E.; Rakich, P. T.; Olsson I I I, R. H.; El-Kady, I.; Phinney, L. M. *Appl. Phys. Lett.* **2009**, *95*, 161902.
(28) McConnell, A. D.; Goodson, K. E. *Annu. Rev. Heat Transfer* **2005**, *14*, 129–168.
(29) McConnell, A. D.; Uma, S.; Goodson, K. E. *J. Microelectromech. Syst.* **2001**, *10*, 360–369.
(30) Mingo, N. *Phys. Rev. B* **2003**, *68*, 113308.
(31) Eucken, A. *Forschung auf dem Gebiete des Ingenieurwesens*; VDI-verlag g.m.b.h.: Dusseldorf, 1932, Ausgabe B, 3/4 VDI Forschungsheft 353.
(32) Prasher, R. *J. Appl. Phys.* **2006**, *100*, No. 034307.
(33) Prasher, R. *J. Appl. Phys.* **2006**, *100*, No. 064302.
(34) Lee, J.-H.; Grossman, J. C.; Reed, J.; Galli, G. *Appl. Phys. Lett.* **2007**, *91*, 223110.
(35) Song, D.; Chen, G. *Appl. Phys. Lett.* **2004**, *84*, 687–689.
(36) Kushwaha, M. S.; Helevi, P.; Martinez, G.; Dobrzynski, L.; Djafari-Rouhani, B. *Phys. Rev. B* **1994**, *49*, 2313–2322.

DOI: 10.1021/nl102918q | *Nano Lett.* **2011,** *11,* 107–112